Unusual High-Frequency Mechanical Properties of Polymer-Grafted Nanoparticle Melts

Mayank Jhalaria,[1] Yu Cang,[2,3] Yucheng Huang,[4] Brian Benicewicz,[4] Sanat K. Kumar,[1,*] and George Fytas[2,†]
[1]Department of Chemical Engineering, Columbia University, New York 10027, New York, USA
[2]Max Planck Institute for Polymer Research, Ackermannweg 10, 55128 Mainz, Germany
[3]School of Aerospace Engineering and Applied Mechanics, Tongji University, 100 Zhangwu Road, Shanghai 200092, China
[4]Department of Chemistry and Biochemistry, University of South Carolina, Columbia 29201, South Carolina, USA

(Received 25 November 2021; revised 20 March 2022; accepted 31 March 2022; published 4 May 2022)

Brillouin light spectroscopy is used to measure the elastic moduli of spherical polymer-grafted nanoparticle (GNP) melts as a function of chain length at fixed grafting density (0.47 chains/nm^2) and nanoparticle radius (8 nm). While the moduli follow a rule of mixtures (Wood's law) for long chains, they display enhanced elasticity and anomalous dissipation for graft chains <100 kDa. GNP melts with long polymers at high σ have a dry zone near the GNP core, surrounded by a region where the grafts can interpenetrate with chain fragments from adjacent GNPs. We propose that the departures from Wood's law for short chains are due to the effectively larger silica volume fraction in the region where sound propagates —this is caused by the short, interpenetrated chain fragments being pushed out of the way. We thus conclude that transport mechanisms (of gas, ions, sound, thermal phonons) in GNP melts are radically different if interpenetrated chain segments can be "pushed out of the way" or not. This provides a facile new means for manipulating the properties of these materials.

DOI: 10.1103/PhysRevLett.128.187801

The addition of inorganic nanoscale fillers to polymers generally yields improvements in mechanical strength, ease of processing, improved temporal stability, and other property sets relative to the neat polymer [1–3]. Unfortunately, most inorganic fillers are immiscible in an organic matrix as the fillers are typically hydrophilic while polymers are apolar. The consequence of such immiscibility on properties is not obvious and generally not controllable. A well-explored method to ensure good nanoparticle (NP) dispersion is by utilizing materials constructed with only polymer-grafted NPs (GNPs) [4]. While the primary aim was to ensure homogenous NP dispersion, such materials display a whole host of unique property sets, e.g., enhanced light gas transport [5–7], ion transport [8,9], phononic and photonic band gap properties [10,11], and impact resistance [12,13].

The underpinning unique feature of these materials is the microstructure of the polymer brush and its interaction with brushes on neighboring GNPs, Fig. 1(a) [14]. Specifically, a recent successful theory shows that a spherical brush in a melt of GNPs can have two regions. The inner dry layer of thickness h_{dry}, with n_{dry} monomers per chain, is comprised of extended chain fragments. This layer is surrounded by an interpenetration region where the remaining segments from each chain, $n_{\mathrm{inter}} = N - n_{\mathrm{dry}}$, are mixed with chain sections from adjacent NPs (N is the total chain length); these interpenetrated chain segments follow Gaussian statistics. The thickness of the interpenetration zone is h_{inter}. To obtain h_{dry}, h_{inter}, n_{dry}, and n_{inter} we use two volume filling conditions: $\frac{4}{3}\pi(R_c + h_{\mathrm{dry}})^3 = \frac{4}{3}\pi R_c^3 + (4\pi \mathrm{R}_c^2 \sigma n_{\mathrm{dry}}/\rho)$, $\frac{4}{3}\pi R_p^3 \equiv \frac{4}{3}\pi(R_c + h_{\mathrm{dry}} + h_{\mathrm{inter}}/2)^3 = \frac{4}{3}\pi R_c^3 + (4\pi R_c^2 \sigma N/\rho)$ where R_c is the core radius of the NP, σ is the grafting density, and ρ is the monomer number density (in units of monomers/nm^3). We also employ the mass balance condition $N = n_{\mathrm{dry}} + n_{\mathrm{inter}}$ and the Gaussian chain assumption $h_{\mathrm{inter}} = n_{\mathrm{inter}}^{1/2} b$ (b is the statistical segment length) for chain segments in the interpenetration zone. This model has been validated against simulation results and it shows that the stretching free energy per chain, $(h_{\mathrm{dry}} + h_{\mathrm{inter}}/2)^2/\mathrm{Nb}^2$ goes through a maximum at $N_{\mathrm{max}} = (2\sqrt{3} + 3)(\rho R_c/\sigma)$ [14–17]. Below this chain length, the brush is dominated by extended brush segments, while it becomes more Gaussian-like for longer chains. While the two zones are structurally different, previous works have indicated that both the dry and interpenetrated regions might be important for mechanical behavior [18–20]. For the particular case of GNP melts, the nature of the mechanical response has been observed to be dependent on probe frequency, e.g., nanoindentation [16,21,22], dynamical mechanical analysis [23], rheology [20,24–26], quartz crystal microbalance [27], and Brillouin light scattering, BLS [19]. While several different reinforcement mechanisms have been proposed [19,22,28,29], the relation between GNP microstructure and mechanical properties is unclear.

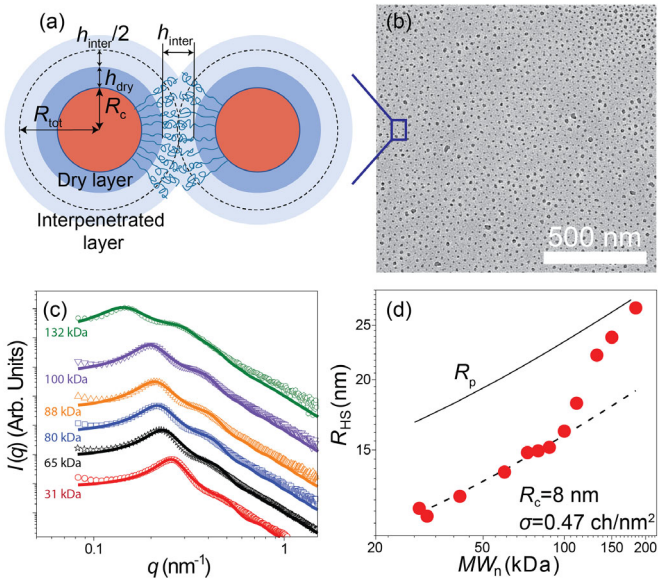

FIG. 1. (a) Schematic of polymer brush structure in GNP assemblies. (b) Transmission electron microscopy (TEM) image for GNP melts with molecular weight $MW_n = 80$ kDa and grafting density $\sigma \approx 0.47$ chains/nm^2. (c) SAXS patterns for GNPs with increasing MW_n (bottom—31 kDa; top—132 kDa, hollow symbols). The data were modeled as a product of a polydisperse hard sphere form factor (with known radius and dispersity) with a monodisperse Percus-Yevick hard sphere structure factor, with two parameters R_{HS} and ϕ_{HS}, the hard sphere radius and volume fraction (solid lines). (d) Estimated GNP radius, R_{HS} (symbols) and theoretically predicted radius $R_p = R_c + h_{dry} + h_{inter}/2$ (solid line, see panel (a); [14]) plotted vs MW_n of the polymer graft. The dashed line is $R_{dry} = R_c + h_{dry}$.

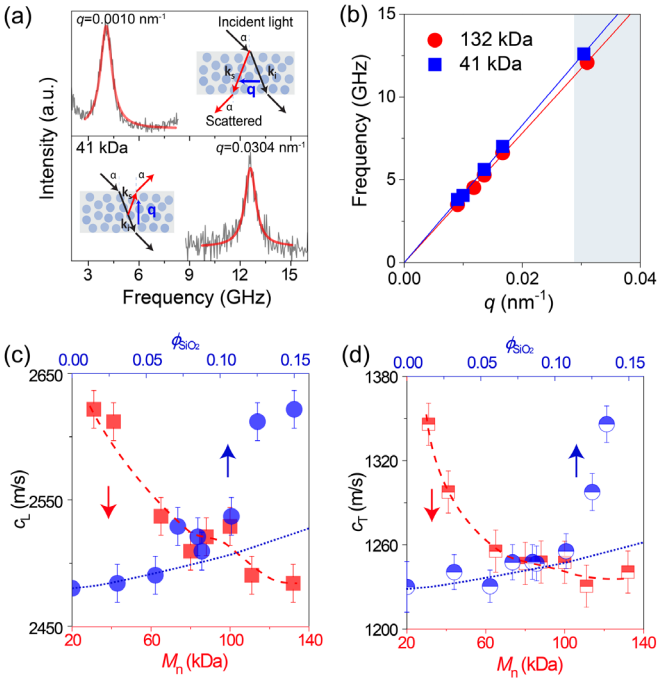

FIG. 2. (a) Anti-Stokes Brillouin light scattering (BLS) spectra at two different scattering wave vectors q's for a representative GNP melt with graft molecular weight, $MW_n = 41$ kDa. The incident angle is α, the phonon wave vector, $\mathbf{q} = \mathbf{k_s} - \mathbf{k_i}$ is defined by the wave vectors of the scattered (k_s) and incident (k_i) light with wavelength λ (=532 nm). The BLS spectra represented (red lines) by single Lorentzian line are recorded at two different q directions: in-plane with $q = 0.001$ nm^{-1} (upper, transmission) and $q = 0.0304$ nm^{-1} (lower panel, reflection geometry). (b) The corresponding acoustic dispersion relation obtained from the BLS spectra in (a), and the shaded blue region indicates the spectra collected in the reflection geometry [lower panel in (a)]. For comparison, the acoustic dispersion relation of $MW_n = 132$ kDa is also shown. (c),(d) Experimental longitudinal c_L (c) and transverse c_T (d) sound velocities for different molecular weights at $\sigma \approx 0.47$ chains/nm^2 for PMA grafted SiO_2 GNP. The blue circle and red square points indicate the trend with ϕ_{NP} (top axis) and MW_n (bottom axis), respectively. The blue dotted line indicate the Wood's law representation of the experimental c_L and c_T vs ϕ_{NP} in (c),(d). Red dashed lines are guides to the eye.

Here BLS is used to quantify the mechanical response of poly(methyl acrylate) (PMA) grafted silica NPs. We systematically varied the graft PMA molecular weight (MW_n) while holding the grafting density, $\sigma \approx 0.47$ chains/nm^2, and the silica core radius ($R_c = 8$ nm) fixed in a series of experiments. BLS has important advantages relative to macroscopic mechanical experiments since it allows for a noninvasive measurement of elastic moduli under zero strain by harnessing the thermal phonons in the material. Further, the selection of the polarization and direction of phonon propagation separately gives us the mechanical properties along the longitudinal and transverse directions. The method is insensitive to material defects due to its submicron resolution and the inherently high frequencies enable the measurement of the elastic moduli compared to the viscoelastic modulus accessible by shear rheometry at low frequencies. While PMA and PMA-g-SiO_2 are above but near the polymer's glass transition temperature ($T_g \approx 291$ K), the segmental relaxation frequency at the measurement temperature (~1 Hz) is far removed from hypersonic frequencies (~GHz). Thus, the PMA segmental dynamics are frozen in the BLS experiment and do not affect the propagation of GHz thermal phonons.

We use the trends in BLS sound velocities as an initial proxy for the elastic mechanical behavior in the GNP assemblies. The BLS spectra from the inelastic scattering of light by the longitudinal and transverse phonons propagating in the medium with wave vector q are depicted in Fig. 2(a). In this case we used a GNP with $MW_n = 41$ kDa for longitudinal phonon propagation in and out of plane [top and bottom insets to Fig. 2(a)] with wave vectors $q = 0.001$ and 0.0304 nm^{-1}, respectively. For all GNPs, only a single longitudinal phonon was visible at all q's, implying that the films are spatially homogenous over a length scale $2\pi/q \sim 200 - 600$ nm defined by the smallest and largest wave vector studied, respectively. This is unsurprising because the size of the building block NPs and

characteristic interparticle spacings (20–45 nm) are about an order of magnitude smaller than the spatial domain probed. Thus, unlike previous studies we do not observe the characteristic vibrational modes and phonon band gaps associated with the first Brillouin zone due to the nanoscopic size of the GNPs used and the short interparticle spacing [10].

All polarized spectra at a given q were represented by a single Lorentzian line shape centered at the phonon frequency, f_0, with a full-width at half-maximum linewidth, Γ_{exp} (see Brillouin light spectroscopy in the Supplemental Material [30]). We start with the transmission geometry for which the magnitude of $q = (4\pi/\lambda)\sin\alpha$ is independent of the material refractive index. The linear acoustic dispersion relation, $f(q)$ [Fig. 2(b)], yields the longitudinal sound velocity, $c_L = 2\pi f/q$ which is anticipated for thick films ($qd \gg 1$) as in the present case ($d \sim 100$ μm) [33]. For spectra collected in the reflection geometry, the relation between sound velocity and frequency depends on the material refractive index, n. Using the sound velocity c_L (determined in the transmission geometry), we calculate a virtually constant n for the GNP films (Fig. S1 [30]). Figure 2(b) shows that the linear slope of f (q) for the low MW_n (= 41 kDa) GNP is steeper than for the higher molecular weight (132 kDa) GNP. Hence, the shorter graft chain GNP possesses a higher c_L value [see also Fig. 2(c)]. This difference is not found in the absence of silica NPs as the measured c_L (=2480 ± 20 m/s) is invariant to variations of MW_n (66 vs 125 kDa) in bulk PMA films. This MW_n independent sound velocity should also apply to the two lower MW_n PMA, since both are well above the entanglement molecular weight (~10 kDa) for bulk PMA.

The longitudinal c_L of the GNPs, depicted in Fig. 2(c), conforms to the effective medium Wood's model [blue dotted line, Eq. (1)] for low ϕ_{NP}, i.e., high MW_n grafts; for the Wood's law representation, we used $c_{L,NP} = 4950$ m/s, $c_{L,PMA} = 2480$ m/s, and density values, $\rho_{\text{NP}} = 2.07$ g/cm^3 and $\rho_{\text{PMA}} = 1.22$ g/cm^3, based on pycnometry measurements [5]. Similarly, the longitudinal modulus, $M = \rho c_L^2$ (ρ is the GNP density) varies linearly with ϕ_{NP}, Fig. 3(a):

$$\frac{1}{M} = \frac{\phi_{\text{NP}}}{M_{\text{NP}}} + \frac{1-\phi_{\text{NP}}}{M_P}. \tag{1}$$

However, the experimental data show a much stronger dependence than the Wood's law predictions for $\phi_{\text{NP}} > 0.05$ corresponding to shorter graft chain lengths ($MW_n \sim 30$ to 80 kDa). Notably, c_L at low MW_n's cannot be captured even if we treat the NP as an infinitely rigid filler with $c_{L,\text{NP}} \to \infty$. Other effective medium theories are also unable to capture the observed behavior [34]. Moreover, c_L seemingly develops a plateau at intermediate molecular weights between 80–100 kDa, as all four values

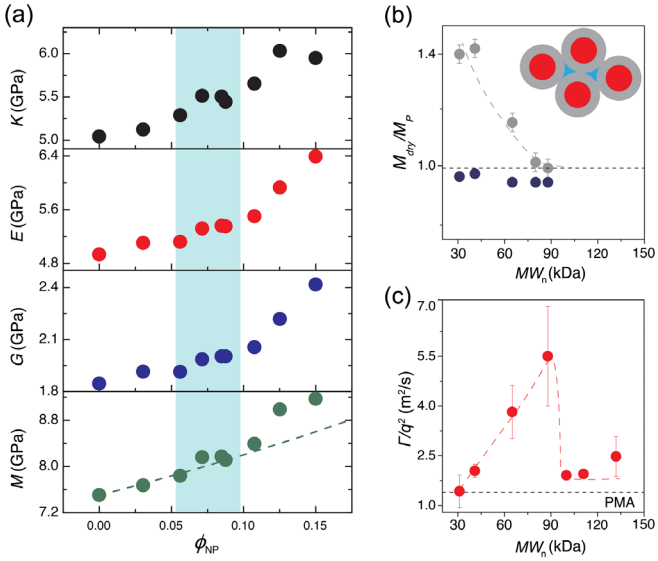

FIG. 3. (a) Bulk (K), Young's (E), shear (G), and longitudinal (M) moduli of GNPs GNP's computed from the sound velocities of Figs. 2(c) and 2(d). The dashed line is the theoretical prediction based on the effective medium Wood's law and the shaded area is for the structural transition. (b) The modulus ratio for the dry region and bulk polymer, M_{dry}/M_P, computed from the Wood's law assuming either a three-layer (core, dry and interpenetrated regions) or closely packed hard sphere (core, dry region) contribution indicated by the gray and blue filled symbols, respectively. In the hard sphere model, the polymer grafts of the interpenetrated region occupy the interstitial (void) regions schematically indicated (in blue) in the inset. Modulus data for chain lengths which deviate from Wood's law are shown in the graph. (c) Hypersonic sound absorption Γ/q^2 in GNPs for different graft MW_n. The black dashed line denotes the sound absorption in the bulk PMA matrix, whereas the red dashed is guide to the eye.

are very similar within experimental error in Fig. 2(c). A similar trend, albeit less pronounced, is also observed for the transverse sound velocity, c_T in Fig. 2(d) indicating a virtually constant c_L/c_T or Poisson's ratio (Fig. S2 [30]).

For a continuum system, the high-frequency longitudinal (M), shear (G), Young's (E), and bulk (K) moduli of GNPs can be computed from the two sound velocities c_L and c_T and the system density (see Brillouin light spectroscopy in the Supplemental Material [30]). The four engineering moduli are shown as a function of ϕ_{NP} in Fig. 3(a). The deviation from the Wood's law [dashed line in Fig. 3(a)] occurs for $\phi_{\text{NP}} > 0.05$ resembling the trend observed for sound velocities [Figs. 2(c) and 2(d)]. Incorporating NPs thus has a beneficial effect on the overall moduli; more importantly, the elastic strength is beyond the trivial effective medium (composition) effect reported for conventional nanocomposites [35,36] in this range of NP loadings (See Fig. S3 [30], for longitudinal modulus data at additional grafting densities).

We elucidated GNP structure using transmission electron microscopy (TEM) and small angle x-ray scattering (SAXS). The SAXS intensity $I(q)$ vs wave vector q of Fig. 1(c) displays a strong peak at a wave vector $q*$, which shifts to lower values with increasing MW_n, consistent with an increase in spacing between the NPs. The interparticle spacing follows $\phi_{\mathrm{NP}}^{-1/3}$ conforming to space filling (Fig. S4 [30]); ϕ_{NP} is estimated from thermal gravimetric analysis (TGA) experiments (Table S1 [30]). While the crude analysis of the SAXS data provides the gross picture of inter-NP spacings, it does not represent the MW_n dependent GNPs microstructure, which is described below.

To this end the SAXS data were analyzed in more detail as a product of a polydisperse hard sphere form factor (with known radius and polydispersity) with a monodisperse Percus-Yevick structure factor, with two parameters R_{HS} and ϕ_{HS}, the hard sphere radius and volume fraction. While the system is not a true hard sphere suspension, it is comprised of only a single component. The adjustable parameter, R_{HS}, represents the mean effective size of a GNP. The volume fraction, ϕ_{HS}, on the other hand, is a convolution of several factors including ϕ_{NP} and space filling of the polymer grafts. The resulting experimentally determined mean size of the NPs, i.e., R_{HS} (symbols) shows good agreement with the R_p estimated from model predictions [solid line in Fig. 1(d)] [14], for $MW_n \gg 100$ kDa. However, for lower MW_n the scattering derived R_{HS} is found to be much smaller and equal to $R_{\mathrm{dry}} = R_{\mathrm{c}} + h_{\mathrm{dry}}$ (the dashed line in Fig. 1(d)). Theory suggests that chains with $MW_n \approx 75$ kDa have maximum stretching; in parallel, rheology [19] suggests that the morphology of the GNP melts transition in the vicinity of $MW_n \approx 100$ kDa. While these differences are likely due to the polydispersity of the NPs, all of the experimental data, including the GNP structure from SAXS, imply that the GNPs undergo a structural transition in the vicinity of $MW_n \approx 100$ kDa. We conjecture that, for shorter chains (extended brush dominated regime), the interpenetration zone is small enough in extent that it can relax and populate the interstitial regions between the GNPs [37–40]. Thus, inter-NP contact, is through adjacent two dry zones [inset to Fig. 3(b)]—this explains why R_{HS} tracks $R_{\mathrm{dry}} = R_c + h_{\mathrm{dry}}$ under these conditions. At higher chain lengths (interpenetrated regime dominated), we find the more expected $R_p \approx R_{\mathrm{HS}}$ implying that the interpenetrated zones are not exclusively occupying the interstitial spaces. We posit that this crossover in behavior of the interpenetrated zone provides key insights into the tuning of the mechanical response in GNPs.

To rationalize the observed system-specific deviation from the effective medium elasticity behavior we first apply the Wood's law with three contributions, from the core ($M_c = 49.7$ GPa), from the interpenetrated zone (modulus equal to that of the bulk polymer, $M_{\mathrm{inter}} = M_p = 7.5$ GPa), and from the dry zone, M_{dry} with known ϕ_{NP}, ϕ_{inter}, and ϕ_{dry} $(=1 - \phi_{\mathrm{NP}} - \phi_{\mathrm{inter}})$ (See Brillouin light scattering in the Supplemental Material [30]). Hence, the only unknown M_{dry} to the experimental moduli for $MW_n \leq 100$ kDa and shown in Fig. 3(b) (gray filled symbols). Expectedly, the enhanced GNP elasticity for $MW_n \leq 100$ kDa can be rationalized by an effective harder "dry" region compared to the bulk polymer [Fig. 3(b)] [18]. However, the value of M_{dry} is molecular weight dependent, which is hard to rationalize. An alternative explanation follows from SAXS measurements, which suggest that for short chains the interpenetration zone fills the interstitial spaces so that NPs with their associated dry brushes come into contact [inset to Fig. 3(b)]. Motivated by this emerging new microstructural picture we propose that sound can propagate through closed packed hard spheres (i.e., a medium with alternating NP cores and dry zones) thus ignoring the interpenetrated zones that populate the voids between the NPs. In an electrical circuit analogy, these interpenetrated domains with smaller moduli are in parallel to the faster sound propagation channel comprised of the NP cores and the dry zones; this is similar in spirit to observations made for AAO templates infiltrated with polymers. [41] With this assumption, the GNP modulus only depends on an effective core volume fraction $\phi_c = [R_c/(R_c + h_{\mathrm{dry}})]^3$ (Table S1 [30]), which is higher than the actual NP volume fraction, ϕ_{NP}, with the remaining space being occupied by the dry zone (1-ϕ_c). Utilizing Eq. (1) for these two contributions, with one unknown parameter, M_{dry}, yields results shown as blue symbols in Fig. 3(b). Notably, M_{dry} is very close but consistently below the polymer modulus; it also is satisfactorily almost independent of molecular weight. These results surprisingly indicate that the dry zone of a polymer brush is a more compressible region relative to the corresponding free polymer. Additional support for this picture comes from the fact that data from a second system with $\sigma \approx 0.65$ ch/nm^2 with varying MW_n follow the same trend when we plot M_{dry}/M_P as a function of ϕ_c [Fig. S5 [30]]. These trends only appear to hold for materials with a well-defined dry zone, lending further credence to these notions; for the system with $\sigma \approx 0.11$ chains/nm^2, there is no dry zone due to the sparse grafting density, and this analysis does not hold.

The phonon dissipation Γ/q^2 is obtained from the experimental BLS spectra [Fig. 2(a)] to examine the relation of the phonon lifetime $(1/\Gamma)$ to the brush microstructure in GNPs. In the absence of hypersonic dispersion, occurring only at temperatures about 150 K above the glass transition T_g [42], the experimental $\Gamma/q^2 = (\Gamma_{\mathrm{exp}} - \Gamma_0)/q^2$ should be q independent, where Γ_0 denotes the instrumental width (Fig. S6 [30]). Moreover, the anticipated phonon scattering by the SiO_2 cores is negligible because both $qR_c \ll 1$ and $\phi_{\mathrm{NP}} \ll 1$. [43] Based on the robust $(\Gamma_{\mathrm{exp}}$-$\Gamma_0)/q^2$ slope, both conditions are expectedly fulfilled. Further, in this high frequency $(\omega\tau)^2 \gg 1$ (τ is the segmental α- relaxation time and ω is the phonon

frequency) limit, $\Gamma/q^2 = \eta/\rho \sim 1/\tau$ and like τ, the kinematic high frequency viscosity is a local segmental property. Therefore, Γ/q^2 should be insensitive to the variation of MW_n of the grafts. On the contrary, Γ/q^2 depicted in Fig. 3(c) is dependent on the MW_n of the grafts—and displays a pinning behavior at $MW_n \approx 88$ kDa and it abruptly approaches the value of bulk PMA for $MW_n > 100$ kDa. A possible explanation would be faster PMA segmental dynamics at the microstructure crossover region caused by local packing changes due to chain extension. Previous studies have shown that fast dynamics in the GHz-THz region are accelerated when compared to the homopolymer and this could explain the more dissipative behavior of the GNPs [44,45]. The fact that the GNPs transition from a dense structure to a liquidlike phase occurs at the same chain MW_n also suggests a possible correlation.

The picture that emerges is radically different from the current understanding of such nanocomposites. A simple application of Wood's law to a three-layer model suggests that the dry zone has a higher modulus than the neat polymer. Rather, we believe that sound propagation apparently predominantly occurs through the NP cores and the dry layer (in series), with a M_{dry}/M_p slightly less than 1. The most important conclusion here is that the departures from Wood's law predictions at low graft chain length are due to the effectively larger silica volume fraction in the region where sound propagates. This is caused by the interpenetrated chains filling interstitial spaces and becoming less relevant to the BLS experiments. This provides a new framework to manipulate the engineering properties of this class of materials and represents the novel contribution of this work.

Financial support for this research was provided by the Department of Energy (Grant No. DE-SC0021272). Y. C. and G. F. acknowledge the financial support by ERC AdG SmartPhon (Grant No. 694977).

*sk2794@columbia.edu
†fytas@mpip-mainz.mpg.de

[1] S. K. Kumar, N. Jouault, B. Benicewicz, and T. Neely, Macromolecules **46**, 3199 (2013).
[2] S. K. Kumar and R. Krishnamoorti, Annu. Rev. Chem. Biomol. Eng. **1**, 37 (2010).
[3] S. K. Kumar, B. C. Benicewicz, R. A. Vaia, and K. I. Winey, Macromolecules **50**, 714 (2017).
[4] N. J. Fernandes, H. Koerner, E. P. Giannelis, and R. A. Vaia, MRS Commun. **3**, 13 (2013).
[5] C. R. Bilchak *et al.*, Macromolecules **50**, 7111 (2017).
[6] C. R. Bilchak *et al.*, ACS Nano **14**, 17174 (2020).
[7] S. P. Jeong *et al.*, ACS Appl. Nano Mater. **4**, 5895 (2021).
[8] S. Choudhury, S. Stalin, Y. Deng, and L. A. Archer, Chem. Mater. **30**, 5996 (2018).
[9] S. Srivastava, J. L. Schaefer, Z. C. Yang, Z. Y. Tu, and L. A. Archer, Adv. Mater. **26**, 201 (2014).
[10] E. Alonso-Redondo, M. Schmitt, Z. Urbach, C. M. Hui, R. Sainidou, P. Rembert, K. Matyjaszewski, M. R. Bockstaller, and G. Fytas, Nat. Commun. **6**, 8309 (2015).
[11] Y. Cang, J. Lee, Z. Wang, J. Yan, K. Matyjaszewski, M. R. Bockstaller, and G. Fytas, Adv. Mater. **33**, 2170013 (2021).
[12] J. Hyon, M. Gonzales, J. K. Streit, O. Fried, O. Lawal, Y. Jiao, L. F. Drummy, E. L. Thomas, and R. A. Vaia, ACS Nano **15**, 2439 (2021).
[13] S. H. Chen, A. J. Souna, S. J. Stranick, M. Jhalaria, S. K. Kumar, C. L. Soles, and E. P. Chan, Soft Matter **18**, 256 (2022).
[14] J. Midya, M. Rubinstein, S. K. Kumar, and A. Nikoubashman, ACS Nano **14**, 15505 (2020).
[15] J. Choi, C. M. Hui, M. Schmitt, J. Pietrasik, S. Margel, K. Matyjazsewski, and M. R. Bockstaller, Langmuir **29**, 6452 (2013).
[16] J. Choi, C. M. Hui, J. Pietrasik, H. C. Dong, K. Matyjaszewski, and M. R. Bockstaller, Soft Matter **8**, 4072 (2012).
[17] K. Ohno, T. Morinaga, S. Takeno, Y. Tsujii, and T. Fukuda, Macromolecules **40**, 9143 (2007).
[18] D. Maillard, S. K. Kumar, B. Fragneaud, J. W. Kysar, A. Rungta, B. C. Benicewicz, H. Deng, L. C. Brinson, and J. F. Douglas, Nano Lett. **12**, 3909 (2012).
[19] J. Midya, Y. Cang, S. A. Egorov, K. Matyjaszewski, M. R. Bockstaller, A. Nikoubashman, and G. Fytas, Nano Lett. **19**, 2715 (2019).
[20] D. Parisi, E. Buenning, N. Kalafatakis, L. Gury, B. C. Benicewicz, M. Gauthier, M. Cloitre, M. Rubinstein, S. K. Kumar, and D. Vlassopoulos, ACS Nano **15**, 16697 (2021).
[21] P. Podsiadlo, G. Krylova, B. Lee, K. Critchley, D. J. Gosztola, D. V. Talapin, P. D. Ashby, and E. V. Shevchenko, J. Am. Chem. Soc. **132**, 8953 (2010).
[22] J. Lee, Z. Wang, J. Zhang, J. Yan, T. Deng, Y. Zhao, K. Matyjaszewski, and M. R. Bockstaller, Macromolecules **53**, 1502 (2020).
[23] Y. Zheng, Z. M. Abbas, A. Sarkar, Z. Marsh, M. Stefik, and B. C. Benicewicz, Polymer **135**, 193 (2018).
[24] E. N. D. Buenning, PhD thesis, E.N.D. Buenning, Columbia University, 2018.
[25] V. Goel, J. Pietrasik, K. Matyjaszewski, and R. Krishnamoorti, Ind. Eng. Chem. Res. **49**, 11985 (2010).
[26] N. Sakib, Y. P. Koh, Y. Huang, K. I. S. Mongcopa, A. N. Le, B. C. Benicewicz, R. Krishnamoorti, and S. L. Simon, Macromolecules **53**, 2123 (2020).
[27] C. R. Bilchak, Y. C. Huang, B. C. Benicewicz, C. J. Durning, and S. K. Kumar, ACS Macro Lett. **8**, 294 (2019).
[28] J. G. Ethier and L. M. Hall, Macromolecules **51**, 9878 (2018).
[29] J. G. Ethier, L. F. Drummy, R. A. Vaia, and L. M. Hall, ACS Nano **13**, 12816 (2019).
[30] See Supplemental Material at http://link.aps.org/supplemental/10.1103/PhysRevLett.128.187801 for sample and experimental details, data at different grafting densities as well as Refs. [5,14,31,32].
[31] C. Li and B. C. Benicewicz, Macromolecules **38**, 5929 (2005).
[32] I. Bressler, J. Kohlbrecher, and A. F. Thunemann, J. Appl. Crystallogr. **48**, 1587 (2015).

[33] W. Cheng, R. Sainidou, P. Burgardt, N. Stefanou, A. Kiyanova, M. Efremov, G. Fytas, and P. F. Nealey, Macromolecules **40**, 7283 (2007).
[34] G. C. Gaunaurd and W. Wertman, J. Acoust. Soc. Am. **85**, 541 (1989).
[35] D. Zhao, D. Schneider, G. Fytas, and S. K. Kumar, ACS Nano **8**, 8163 (2014).
[36] E. Schechtel, Y. P. Yan, X. F. Xu, Y. Cang, W. Tremel, Z. Y. Wang, B. W. Li, and G. Fytas, J. Phys. Chem. C **121**, 25568 (2017).
[37] P. Agarwal, S. A. Kim, and L. A. Archer, Phys. Rev. Lett. **109**, 258301 (2012).
[38] Y. Wei, Y. F. Xu, A. Faraone, and M. J. A. Hore, ACS Macro Lett. **7**, 699 (2018).
[39] A. Sharma, M. Kruteva, M. Zamponi, S. Ehlert, D. Richter, and S. Förster, Phys. Rev. Mater. **6**, L012601 (2022).
[40] Y.-G. Kim, M. Wagner, and H. Thérien-Aubin, Macromolecules **53**, 844 (2020).
[41] A. Sato, Y. Pennec, N. Shingne, T. Thurn-Albrecht, W. Knoll, M. Steinhart, B. Djafari-Rouhani, and G. Fytas, ACS Nano **4**, 3471 (2010).
[42] P. Voudouris, N. Gomopoulos, A. Le Grand, N. Hadjichristidis, G. Floudas, M. D. Ediger, and G. Fytas, J. Chem. Phys. **132**, 074906 (2010).
[43] D. O. Riese and G. H. Wegdam, Phys. Rev. Lett. **82**, 1676 (1999).
[44] M. Jhalaria, E. Buenning, Y. Huang, M. Tyagi, R. Zorn, M. Zamponi, V. Garcia-Sakai, J. Jestin, B. C. Benicewicz, and S. K. Kumar, Phys. Rev. Lett. **123**, 158003 (2019).
[45] M. Jhalaria, Y. Huang, E. Ruzicka, M. Tyagi, R. Zorn, M. Zamponi, V. García Sakai, B. Benicewicz, and S. Kumar, Macromolecules **54**, 6968 (2021).